UC Davis
UC Davis Previously Published Works

Title

Characterization of densified fully stabilized nanometric zirconia by positron annihilation spectroscopy

Permalink

https://escholarship.org/uc/item/7743f20w

Journal

Journal of Applied Physics, 99(2)

ISSN

0021-8979

Authors

Garay, J E
Glade, S C
Asoka-Kumar, P
et al.

Publication Date

2006

Peer reviewed

Characterization of densified fully stabilized nanometric zirconia by positron annihilation spectroscopy

J. E. Garay[a)]
Department of Chemical Engineering and Materials Science, University of California, Davis, California 95616

S. C. Glade and P. Asoka-Kumar
Lawrence Livermore National Laboratory, Livermore, California 94550

U. Anselmi-Tamburini and Z. A. Munir[b)]
Department of Chemical Engineering and Materials Science, University of California, Davis, California 95616

Fully stabilized nanometric zirconia samples with varying degrees of porosity and grain sizes were analyzed using the coincidence Doppler broadening mode of the positron annihilation spectroscopy (PAS). A decrease in the low-momentum fraction was observed and coincided with a decrease in porosity. In addition to pores, it is proposed that defects in the negatively charged grain-boundary space region act as positron trapping centers; their effectiveness decreases with an increase in grain size. It is shown that PAS is sensitive to small grain-size differences within the nanometric regime in these oxide materials. © *2006 American Institute of Physics*. [DOI: 10.1063/1.2163016]

I. INTRODUCTION

Nanocrystalline oxide ceramics have attracted considerable attention in the past few years for both scientific and technological reasons. The presence of a large fraction of atoms in the grain-boundary region significantly alters the physical and mechanical properties of the material.[1] Interest in oxide ceramics has been motivated by potential applications as electro- and optoceramics. The former is driven by utilization in high-temperature fuel cells, and the latter in high-intensity discharge lamps, luminescent tubes, and lasers.

The development of more efficient methods for the synthesis of high-purity nanocrystalline oxide powders has prompted efforts aimed at consolidating the powders to form useful ceramics. The challenge is to do this and still maintain the nanostructure, avoiding significant grain growth at the typically high temperatures needed for consolidation. Preparing fully dense nanocrystalline oxides with crystallite size of <30 nm is not easily achieved because of the attendant growth in the size of the crystallites during such processes as sintering or hot pressing.

A technique that has shown some promise in the consolidation of nanostructured materials is the spark plasma sintering (SPS) method.[2–4] The technique has been used recently to consolidate nanocrystalline fully stabilized zirconia.[5,6] The method is similar to conventional hot pressing, but in the SPS case all of the energies for the process come from high-intensity current pulses applied to a graphite die containing the sample. The primary effect is Joule heating but other effects, such as current-enhanced mass transport and reactivity, are believed to contribute to the process.[7]

Using the positron annihilation technique (PAS), we have investigated the sintering process and the resulting nanostructured fully stabilized zirconia and we report the results in this paper. The PAS technique has been widely used to study the occurrence of defects and their evolution in a variety of solids.[8] Its ability to detect lattice defects (particularly point defects), which cannot be detected by other means, has contributed to its success as a nondestructive tool. PAS takes advantage of the fact that positively charged positrons tend to localize in open-volume regions where there are missing positively charged atomic nuclei.[9] Subsequently, the "trapped" positrons annihilate with electrons in the area, giving off information about the annihilation site. The information is in the form of gamma rays (positron-electron annihilation produces primarily two 511 keV gamma rays) traveling in opposite directions. By simultaneously recording the energies of these gamma rays, coincidence Doppler broadening (CDB) mode of PAS extends the sensitivity of the annihilation spectra to higher-momentum values and allows the exploration of contributions from different chemical species.[10] Positron overlap with high-momentum electrons (which are dominated by electrons that retain atomic character even when embedded in a solid) can be used for identification of the chemical species associated with the trapped sites.

The PAS technique has been used previously for characterizing ceramics,[11–15] including zirconia.[16–19] The positron annihilation lifetime spectroscopy (PALS) mode has been the most commonly used, but the angular correlation of the annihilation radiation (ACAR) and Doppler broadening have been used as well. Yagi *et al.*[16] studied the sintering behavior of partially stabilized zirconia (PSZ, 2 mol % yttria ZrO_2) nanopowders (~100 nm agglomerates of smaller particles)

[a)]Present address: Department of Mechanical Engineering, University of California, Riverside, CA 92521.
[b)]Author to whom correspondence should be addressed; electronic mail: zamunir@ucdavis.edu

99, 024313-1

with the PALS technique. They showed that sintering of PSZ takes place via processes occurring in three separate temperature ranges: (a) $T < 800\,^\circ\text{C}$, where intra-agglomerate nanovoids begin to disappear; (b) $T = 800-1200\,^\circ\text{C}$, where intra-agglomerate nanovoids are eliminated; and (c) $T > 1200\,^\circ\text{C}$, where the inter-agglomerate micropores are eliminated. The interaction of positrons with point defects and grain boundaries in zirconia has also been investigated by PAS.[17–19] This interaction is particularly complex as the main point defects (oxygen vacancies) and the grain-boundary cores are both characterized by a fairly strong positive charge that reduces the probability of interaction with positrons. The authors suggested that defect associates, characterized by neutral charge, can play an important role in the interaction of zirconia samples with positrons.

The effect of grain size on the results of PAS analyses was investigated by Massoud *et al.* for $BaTiO_3$.[12] They found that increasing the grain size from 1–2 to 100 μm decreased the average positron lifetime in the samples, which was attributed to positron trapping at grain boundaries. Furthermore, the authors demonstrated the effectiveness of the PAS technique in identifying the dopant species in $BaTiO_3$.

There are very few reported positron annihilation spectroscopy experiments on dense nanocrystalline ceramics. In a study using ACAR measurements on CuO compacts,[14] it was reported that an increase in the low-momentum fraction annihilations (associated with an increase in the open-volume signal) seen in nanometric samples (15–90 nm) was attributed to positron trapping at grain boundaries. In another study on nanocrystalline SnO_2 compacts by Shek *et al.*,[15] the average positron lifetime decreased with increasing sintering temperature, an observation attributed to the elimination of grain boundaries by grain growth during the sintering process.

II. EXPERIMENTAL PROCEDURE

A. Sample preparation

A commercially available fully stabilized zirconia (8 mol % yttria) nanopowder (Tosoh TZ-8Y, Tosoh Co. Tokyo, Japan) with a reported grain size of 21 nm was used in this study. The powders were loaded into graphite dies and sintered in a SPS apparatus (Dr. Sinter 1050, Sumitomo, Tokyo, Japan). The samples were sintered under varying conditions of pressure (17–141 MPa), temperature (900–1600 °C), and holding times (0–16 min). Disk-shaped samples with a diameter of 19 mm and a thickness of 2–3 mm were consolidated to relative densities ranging from ~60% to 100%. The density was determined using the Archimedes method for samples with densities higher than 85%. For samples with higher porosity, densities were calculated from weight and geometric measurements.

B. Microstructural characterization

Microstructural characterization of the samples was made using a high-resolution scanning electron microscopy (SEM) (Philips XL30s) equipped with a field-emission gun and operated at 5 kV and 180 nA. Average grain size was obtained from SEM images of fracture surfaces through the

software ANALYSIS (Soft Imaging System Corp. Lakewood, CO). The results obtained by this method agreed well with values obtained from x-ray-diffraction analyses. X-ray powder diffraction (XRPD) analyses were performed using a Philips 1710 diffractometer equipped with a copper anode operated at 40 kV and 35 mA, graphite curved monochromator on the diffracted beam, and a proportional counter. The crystallite sizes were determined through analyses of XRD line broadening, using a published program[20,21] with sintered silicon used as a standard.

C. Positron annihilation spectroscopy

The sintered zirconia samples were characterized using PAS. A single crystal of fully stabilized zirconia (ZrO_2 +9.5% yttria, Alfa Aesar, MA, USA) and a well-annealed zirconium metal sample were measured as standard materials.

In PAS, a positron annihilates (mass converted to energy) with an electron, predominately yielding two ~511 keV photons traveling in opposite directions, which carry information about the annihilation site. The momentum of the electron-positron pair prior to positron annihilation causes a blueshift and a redshift (Doppler broadening) in the two 511 keV photons. The energy shift of each of the two photons is given by

$$\Delta E = \frac{1}{2}p_L c, \tag{1}$$

where p_L is the longitudinal momentum shift and c is the speed of light. The shifts of the two photons are measured simultaneously in CDB, a specific PAS experimental technique. Each element has its own characteristic orbital electron momentum spectrum, and a determination of the chemical identity of the elements in the positron annihilation site can be obtained. In addition, two convenient parameters can be extracted from the CDB data, the low-momentum fraction (LMF) (frequently referred to as S parameter in the positron literature and defined as part of the annihilation spectra with $p_L < 0.38$ a.u.) and the high-momentum fraction (referred as to W and defined as annihilations with 2.0 a.u. $< p_L < 3.0$ a.u.).

PAS measurements were performed at the Lawrence Livermore National Laboratory (LLNL) using a CDB apparatus. These experiments were preformed using a two-detector setup similar to the one described in a previous work.[10] With this setup, a 1 T magnetic field focuses positrons from a [22] Na source into an ~3-mm-diam spot. Positrons emitted from ^{22}Na sources have energies up to 546 keV, giving a typical implantation depth of the positrons into materials of up to $30-100$ μm. The low-momentum fractions were found using events up to 0.38 a.u.

III. RESULTS

Figure 1 shows the CDB spectra for samples sintered at different temperatures using the same holding time (5 min) and applied pressure (141 MPa). The spectra have been normalized to a single crystal of fully stabilized zirconia [Fig. 1(a)], and to zirconium metal [Fig. 1(b)]. Data for a well-
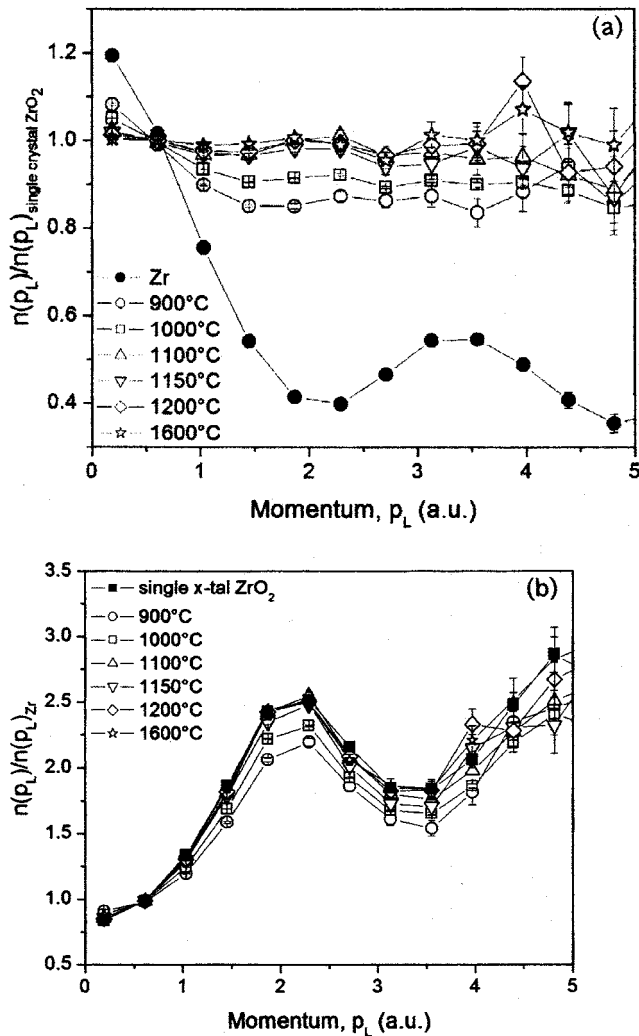
FIG. 1. Coincidence Doppler broadening (CDB) spectra for samples sintered at various temperatures with a holding time of 5 min, heating rate of 200 °C min⁻¹, and applied pressure of 141.1 MPa. (a) Ratios taken with the measured single-crystal zirconia sample. Data for pure Zr are plotted for comparison. (b) Ratios taken with the measured pure Zr sample.

FIG. 2. (a) Low-momentum fraction vs sintering temperature for ZrO$_2$. Samples are held at temperature for 5 min. The heating rate is 200 °C min⁻¹ and the applied pressure is 141.1 MPa. A measured value for single-crystal zirconia is plotted for comparison. (b) Changes of relative density and grain size with sintering temperature for the samples of Fig. 1(a).

annealed pure zirconium sample and for the zirconia are plotted in Figs. 1(a) and 1(b), respectively. As mentioned previously, the low-momentum ($< \sim 2$ a.u.) part of the spectrum is due to valence electrons while the higher-momentum shifts are caused by core electrons.[10] In addition, the very low-momentum parts reveal the relative concentration of defects. Inspection of Fig. 1 reveals that the samples reacted at lower temperatures have significantly higher low-momentum parts (<0.6 a.u.) than the single crystal.

Figure 2(a) shows the variation of LMF with sintering temperature for samples sintered using 141 MPa with a 5 min holding time at temperature. The low-momentum fraction decreases markedly with increasing temperature. A fully stabilized zirconia single crystal was also measured and its low-momentum value is included for comparison. The change in density and crystallite size accompanying this thermal treatment is shown in Fig. 2(b) for the same samples.[5] It is noted that the marked decrease in the LMF (in the range of 900–1200 °C) coincides with a marked change in density over the same temperature range. In contrast, the change in
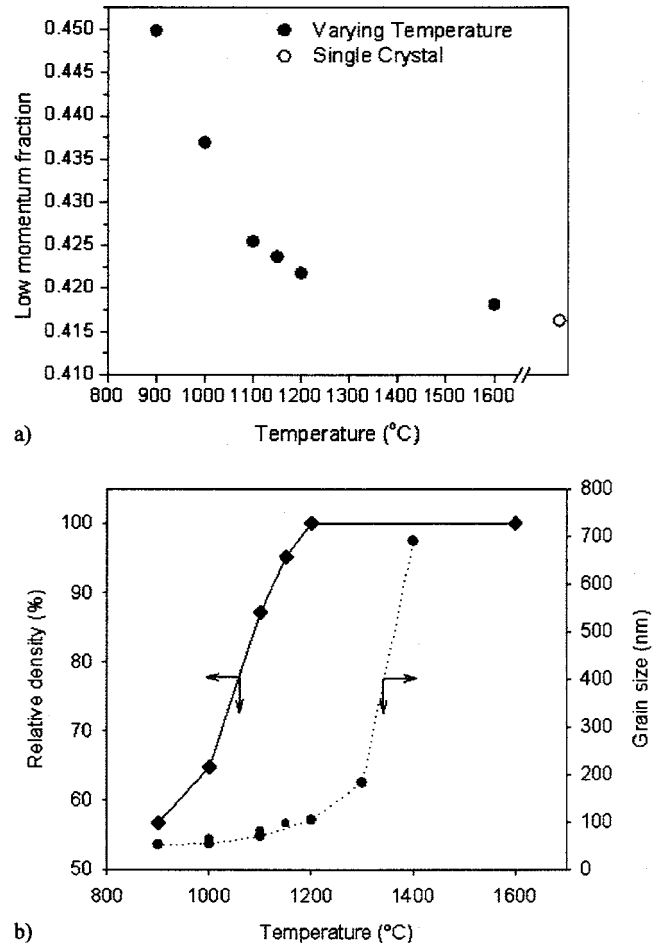
crystallite size is relatively small over this temperature range, becoming important only when the temperature exceeds 1200 °C where the relative density reaches 100%.

Figure 3(a) shows the change in LMF for samples sintered for different times at a constant temperature (1200 °C) and pressure (141 MPa). As Fig. 3(b) shows, the samples reach full density only after a 2 min hold. The grain size increases significantly up to the time the sample is fully dense and then increases at a lower rate after that. Figure 4(a) shows the change in the LMF for the samples sintered at 1200 °C for 5 min with different values of applied pressure. The results show a significant decrease in the LMF with increasing applied pressure. This corresponds with the large change in relative density resulting from an increase in pressure, as can be seen from Fig. 4(b). It is important to note that there is basically no effect of the pressure on crystallite size. Thus the changes in LMF are primarily the consequence of densification. The relationship between relative density and LMF of these samples is depicted in Fig. 5. A similar trend (although with a different scale) between LMF and crystallite size is seen in Fig. 6 for the samples sintered at the same temperature (1200 °C). All of the samples represented
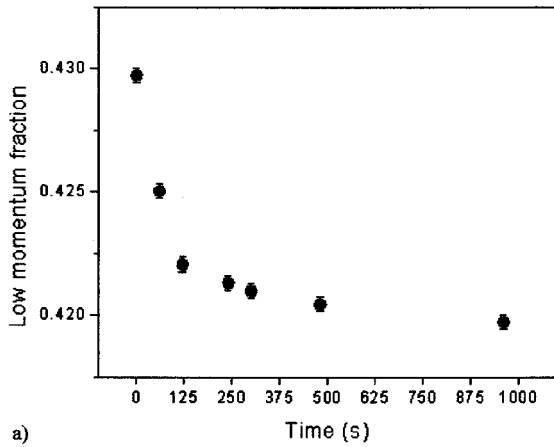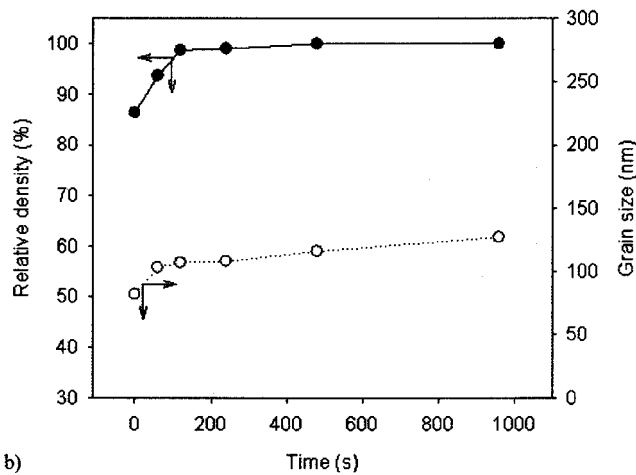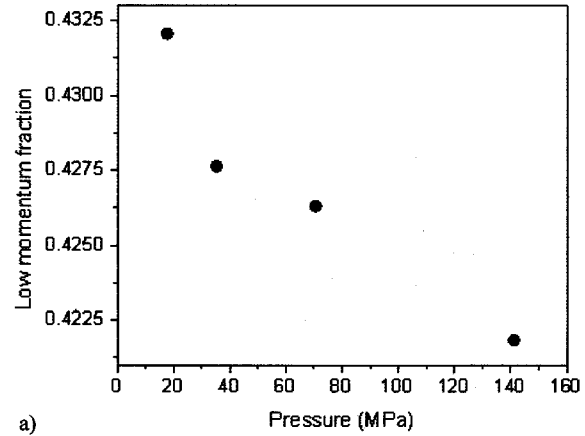
FIG. 3. (a) Low-momentum fraction as a function of sintering time at 1200 °C. Heating rate: 200 °C min^{-1}; applied pressure: 105.8 MPa. (b) Changes of relative density and grain size with sintering time at 1200 °C for the samples of Fig. 3(a).

FIG. 4. (a) Low-momentum fraction as a function of applied pressure for ZrO$_2$ samples sintered at 1200 °C for 5 min. Heating rate: 200 °C min^{-1}. (b) Effect of pressure on relative density and grain size for the samples of Fig. 4(a).
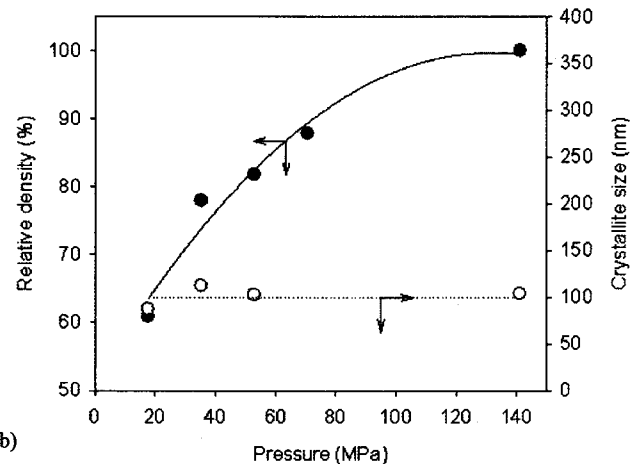
in this figure are fully dense (over 99% theoretical density). The low-momentum fraction decreases with increasing grain size.

IV. DISCUSSION

The different types of defects in sintered zirconia which can contribute to the PAS results include point defects, grain boundaries, and pore volumes. Point defect equilibria in zirconia are quite complex with several different defects and their associated entities. The main defects in bulk zirconia are represented by substitutional yttrium and by oxygen vacancies (Y'_{Zr} and $V^{\bullet\bullet}_O$ in the Kröger-Vink notation[22]). Due to their strong positive charge, $V^{\bullet\bullet}_O$ are not likely to attract positrons. However, it has been shown that at low temperatures only a relatively small fraction of free oxygen vacancies are present as unassociated. The majority tends to be present as associated with substitutional yttrium ($Y'_{Zr}V^{\bullet\bullet}_O$).[23,24] This associated defect tends to be dominant at low concentration of yttrium, while with higher concentration more complex associates, e.g., ($Y'_{Zr}V^{\bullet\bullet}_OY'_{Zr}$), become dominant. These associated defects have a low (or no) positive charge and so can interact with positrons. Other possible defects with a negative charge, such as V''''_{Zr}, occur in very low concentrations and thus can be ignored.

Grain boundaries can play a major role in PAS of nanometric materials. The typical positron diffusion length L_+ in solids is on the order of ≈ 300 nm.[8] Thus in nanocrystalline materials (with grain sizes <100 nm), trapping of positrons at the grain boundaries as well as other open-volume sites is
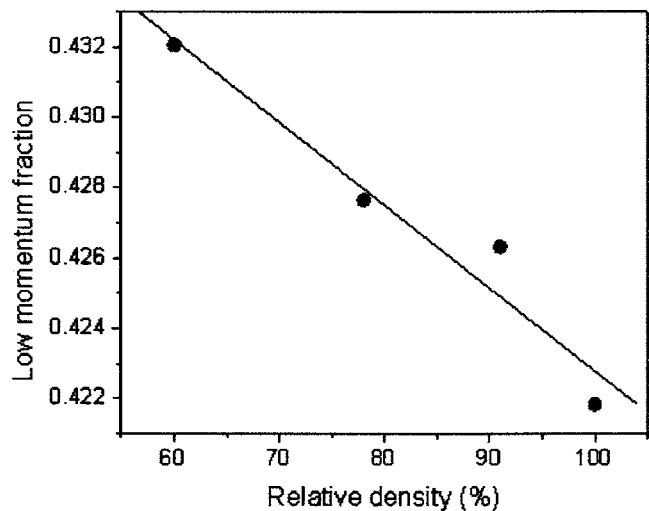

FIG. 5. Low-momentum fraction vs % theoretical density of sintered ZrO$_2$ samples with constant grain size.
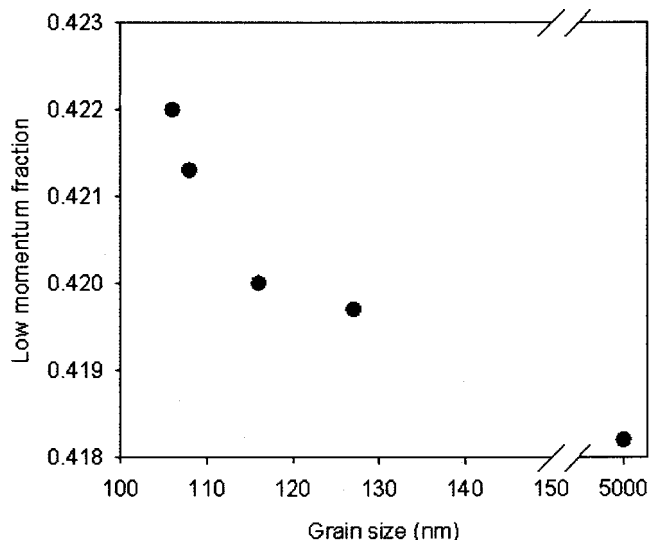
FIG. 6. Low-momentum fraction vs grain size of fully dense sintered samples.

possible. Schaefer *et al.*[25] reported that crystal interfaces are the primary positron traps in nanocrystalline metals. However, in ionic materials the structure of the grain boundary can be quite complex.[26,27] In such ionic materials, the grain-boundary core is characterized by a fairly strong positive charge with a concomitant (negatively charged) space-charge region extending several nanometers away from the grain-boundary core. Because of the positive charge, the grain boundary is expected to repel positrons. For this reason it is has been suggested that in these materials PAS is not able to provide information on the density of grain boundaries[17,18] in zirconia. On the other hand, it is well established that nanopores can be effective trapping centers for positrons.[11,28] In insulating materials positrons are probably trapped in the form of orthopositronium (*o*-ps). Pores of at least 0.3 nm in size are believed to be required in order to have an efficient trapping of *o*-ps. Large pores also trap positrons but one cannot distinguish a large pore from free surfaces so they do not alter the CDB signal significantly.

The CDB spectra of Fig. 1(a) can be used to infer the positron annihilation sites in the samples. The general shape of the ratio curves is similar for all the sintered samples. However, their relative position is inverted at a momentum value of ~0.6 a.u. Below about 0.6 a.u. the ratio is higher for the low-temperature sintered samples, and decreases with increasing sintering temperature. Above about 0.6 a.u., the ratio is highest for samples sintered at the highest temperature. Since the low-momentum values are indicative of annihilation at defects (in this case, pores), the results at <0.6 a.u. show a decrease with increasing sintering temperature, consistent with a decrease in porosity. On the other hand, ratios at momentum values >0.6 a.u. are indicative of annihilation at core electrons and their values increase with a decrease in porosity, approaching the values obtained for a single crystal of ZrO_2, at ratio of 1, as seen in Fig. 1(a). Similar CDB curve shapes are observed in metals containing vacancies and/or voids, with a larger number density of vacancies/voids giving a higher signal in the low-momentum region, and a

lower, relatively flat signal in the high-momentum region. The observed behavior in the ZrO_2 samples is primarily due to the higher sintering temperatures yielding samples with a lower number density of open-volume defects (i.e., specimens increasing in density with increasing sintering temperature). For sintering temperatures greater than 1100 °C, the CDB curves are almost a straight line at 1.0, indicating that most open-volume positron annihilation sites have been removed from the nanocrystalline compacts at these sintering temperatures.

In addition, Fig. 1(a) shows that the ratio curve for pure Zr is distinctly different from the ZrO_2 curves, suggesting that the predominant annihilation sites in the bulk areas (core electrons) of the sintered samples are near oxygen, not zirconium. This proposal is strengthened when the results are normalized to pure Zr. Figure 1(b) shows a distinct peak at a momentum value of ~2 a.u., which is consistent with prior PAS observations on oxides. The peak is known to be characteristic of annihilations with oxygen in the lattice[29] (as opposed to the metal on the lattice). It is worth emphasizing that in this high-momentum regions annihilations are with core electrons and therefore not caused by open volume.

The dependence of low-momentum fraction on the different experimental parameters also provides an insight on the nature of the annihilation sites. As mentioned previously, the LMF is equivalent to the *S* parameter that is frequently quoted in Doppler broadening studies. LMF data are usually directly attributed to changes in open volume in the samples. Examination of Figs. 2(a) and 2(b) shows that the largest decrease in LMF occurred between 900 and 1200 °C, a decrease that coincided with the marked increase in density. During this range, however, the grain size increased by a relatively small increment, from about 55 to 100 nm. The increase in grain size becomes substantial in the temperature range of 1200–1400 °C, where an increase of a factor of 7 is seen. Over this range, however, the decrease in LMF is relatively small. These observations imply that the most significant cause of the decrease in LMF is the elimination of pores by sintering. Similar observations were made by Yagi *et al.* in a lifetime PAS study on partially stabilized zirconia.[11] These authors concluded that in the range of 800–1200 °C the change in the PAS parameters is related to the disappearance of the intra-agglomerate nanovoids.

The decrease in LMF attributed to grain-size change, although relatively small in comparison with that accompanying void disappearance, is nevertheless of interest in the present work. The possibilities suggested by these observations include the annihilation of positrons at (a) grain boundaries, (b) space-charge region, and (c) nanovoids. In general, grain-boundary cores are open-volume sites and are therefore possible positron traps. From studies on the grain-boundary enrichments with di- and trivalent impurities (and the lack of it with tetra- and pentavalent impurities), it has been concluded that the charge on the core of the grain boundary is positive.[27,30] This would reduce the role of the core region of the grain boundary as a trapping center for positrons. On the other hand, the negatively charged space-charge region (with low oxygen vacancy concentration and a correspondingly high yttrium-ion concentration) is a likely trapping region for

positrons. The effect of changing the grain size on trapping thus depends on the changes of the space-charge region with grain size.

Guo calculated the oxygen vacancy concentration profiles within the space-charge region in doped zirconia as a function of grain size.[31] The profiles of the oxygen concentration showed little change as the grain size was decreased from infinite (single crystal) to about 100 nm,[31] but the change became significant with further decrease in grain size. We would therefore anticipate trapping effects in the space-charge region to be relatively significant as the grain size of our samples increased from about 50 to 100 nm and become less significant as the grain size increased further [to about 700 nm Fig. 2(b)]. This is indeed seen by the relatively small change in LMF between 1200 and 1400 °C as the value approaches asymptotically the value of a single crystal. These results would thus suggest that the marked decease in the LMF between 900 and 1200 °C (Fig. 2(a)] is due to a combination of a decease in porosity and an increase in grain size. Examination of Figs. 4(a) and 4(b) provides support for this conclusion. It should be recalled that the results in this figure represent samples which were sintered at a constant temperature (1200 °C) but under different pressures. The grain size remained constant while the relative density increased markedly from about 60% to 100%. A decrease in LMF of about 0.010 is seen over this density range. From Fig. 2(a), the corresponding change in LMF for the same density range is about 0.025. In this case, however, the grain size was not constant and thus the decrease in LMF is due to both porosity elimination and grain-size growth.

The significant effect of grain size (independent of density) on LMF is most easily appreciated in Fig. 6. Recall that all of the samples in this figure are fully dense (over 99% theoretical density). The observed low-momentum fraction difference is 2.25×10^{-3}. To put this change in perspective, note that slope of the line in Fig. 5 (porosity dependence) is -2.351×10^{-4}. Therefore the LMF change due to grain size is equivalent to a LMF difference corresponding to a 10% increase in relative density. It is worth emphasizing that the density differences in the samples in Fig. 6 are negligible. This effect is attributed to increased positron trapping in the grain-boundary-related space-charge region due to defect equilibrium changes with grain size. This conclusion is strengthened by previous impedance measurements where we directly measured significant changes of specific grain-boundary conductivities[6] on some of the same samples in this study.

The calculations carried out by Guo suggest that the concentration of O vacancies in the space-charge layer varies with grain size.[31,32] As a consequence the author concludes that the charge of the layer varies with grain size. It can be inferred therefore that the defect equilibria associated with the grain boundary can vary with grain size. In this light it may be possible that the positive potential of the grain-boundary core is decreased, i.e., that there are fewer positively charged defects when the grain diameter decreases. This would increase positron annihilation in the grain boundary and is an alternate (although related) explanation for our observed results of LMF dependence on grain size.
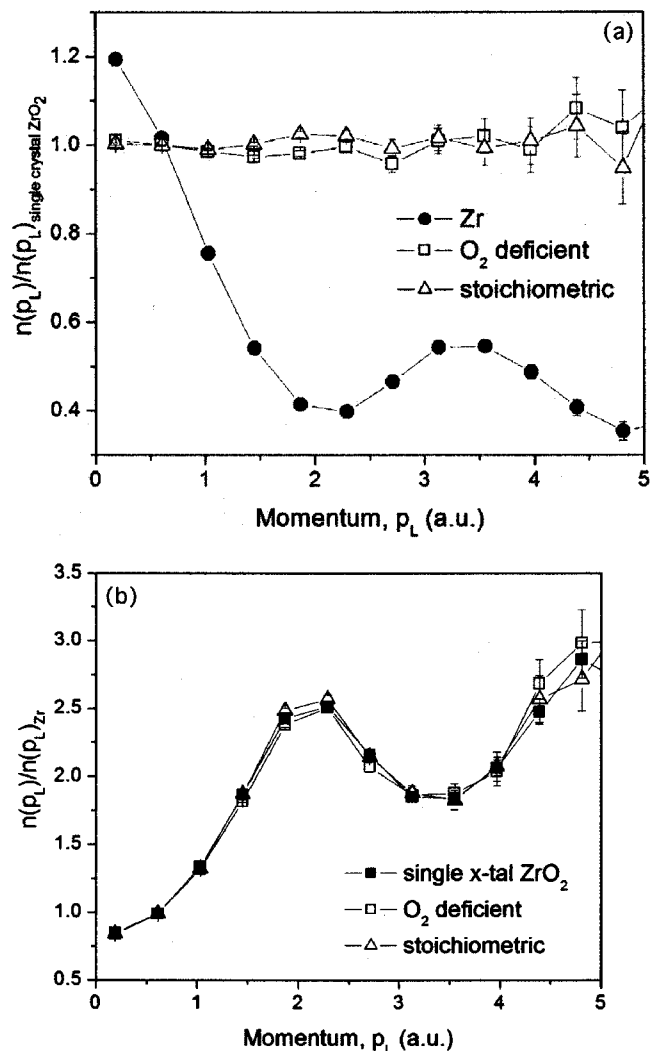

FIG. 7. Coincidence Doppler broadening (CDB) spectra for samples with varying oxygen stoichiometry. (a) Ratios relative to single crystal of ZrO_2. (b) Ratios relative to Zr.

The sintering of zirconia in the SPS has been previously shown to result in changes in the stoichiometry caused by the low oxygen partial pressure inside the graphite.[6] Samples sintered at 1100 °C and higher showed a discoloration indicative of loss of oxygen. To assess whether such a stoichiometric change influenced the PAS results, we conducted experiments on as-sintered and annealed samples. The samples were first sintering in the SPS at 1600 °C. The resulting samples were black in color and had a density of 100% and a grain size of 5 μm. Orbital momentum measurements were made on these samples and they were subsequently annealed in air at 800 °C in order to recover full oxygen stoichiometry. These two conditions represent "extreme" cases with respect to oxygen stoichiometry, while the density and grain size were not changed. The air annealing was done at a temperature too low to affect grain-size changes. The results, presented in Fig. 7(a), show that the spectra from both samples are nearly identical indicating that the stoichiometric change did not play a significant role in the PAS results obtained in this study. The results are also identical when the ratio to Zr

is plotted [Fig. 7(b)], indicating that the annihilation at oxygen ions with core electrons is the same for samples with different oxygen stoichiometry.

V. CONCLUSIONS

Changes in porosity and crystallite size during sintering of fully stabilized nanometric zirconia samples were analyzed by the coincidence Doppler broadening mode of the positron annihilation spectroscopy (PAS). A decrease in the low-momentum fraction was observed and coincided with a decrease in porosity and to a lesser extent with an increase in crystallite size. The effect of crystallite size is believed to relate to the role of the negatively charged grain-boundary space regions as positron trapping centers. PAS can therefore be used to detect grain-boundary-related defects and subsequently grain-size changes in stabilized zirconia.

ACKNOWLEDGMENTS

[1] C. Suryanarayana and C. Koch, Hyperfine Interact. **130**, 4 (2000).

[2] M. Tokita, J. Soc. Powder Technol. Jpn. **30**, 790 (1993).

[3] Z. Shen, Z. Zhao, H. Peng, and M. Nygren, Nature (London) **417**, 266 (2002).

[4] M. Omori, Mater. Sci. Eng., A **A287**, 183 (2000).

[5] U. Anselmi-Tamburini, J. E. Garay, Z. A. Munir, A. Tacca, F. Maglia, G. Spinolo, and G. Chiodelli, J. Mater. Res. **19**, 3255 (2004).

[6] U. Anselmi-Tamburini, J. E. Garay, Z. A. Munir, A. Tacca, F. Maglia, G. Spinolo, and G. Chiodelli, J. Mater. Res. **19**, 3263 (2004).

[7] U. Anselmi-Tamburini, J. E. Garay, and Z. A. Munir, Mater. Sci. Eng., A **407**, 24 (2005).

[8] T. E. M. Staab, R. Krause-Rehberg, and B. Kieback, J. Mater. Sci. **34**, 3833 (1999).

[9] M. J. Puska and R. M. Nieminen, Rev. Mod. Phys. **66**, 841 (1994).

[10] P. Asoka-Kumar, M. Alatalo, V. J. Ghosh, A. C. Kruseman, B. Nielson, and K. G. Lynn, Phys. Rev. Lett. **77**, 2097 (1996).

[11] Y. Yagi, S. Hirano, Y. Ujihira, and M. Miyayama, J. Mater. Sci. Lett. **18**, 205 (1999).

[12] A. M. Massoud, R. Krause-Rehberg, H. T. Langhammer, J. Gebauer, and M. Mohsen, Mater. Sci. Forum **363–365**, 144 (2001).

[13] J. Ghosh, J. Vinita, B. Nielsen, and T. Friessnegg, Phys. Rev. B **61**, 207 (2000).

[14] A. P. Druzhkov, B. A. Gizhevskii, V. L. Arbuzov, E. A. Kozlov, K. V. Shalnov, S. V. Naumov, and D. A. Perminov, J. Phys.: Condens. Matter **14**, 7981 (2002).

[15] C. H. Shek, J. K. L. Lai, and G. M. Lin, J. Phys. Chem. Solids **60**, 189 (1999).

[16] Y. Yagi, S. Hirano, M. Miyayama, and Y. Ujihira, Mater. Sci. Forum **255–257**, 433 (1997).

[17] X. Guo, J. Mater. Sci. **15**, 2017 (1996).

[18] Z. Wang, Z. Q. Chen, J. Zhu, S. J. Wang, and X. Guo, Radiat. Phys. Chem. **58**, 697 (2000).

[19] X. Guo and Z. Wang, J. Eur. Ceram. Soc. **18**, 237 (1998).

[20] S. Enzo, G. Fagherazzi, A. Benedetti, and S. Polizzi, J. Appl. Crystallogr. **21**, 536 (1988).

[21] A. Benedetti, G. Fagherazzi, S. Enzo, and M. Battagliarin, J. Appl. Crystallogr. **21**, 543 (1988).

[22] F. A. Kröger, *Chemistry of Imperfect Crystals* (North Holland, Amsterdam, 1974), Vol. 2.

[23] V. Butler, C. R. A. Catlow, and B. E. F. Fender, Solid State Ionics **5**, 539 (1981).

[24] E. C. Subbarao and H. S. Maiti, Solid State Ionics **11**, 317 (1984).

[25] H. E. Schaefer, R. Wurschum, R. Birringer, and H. Gleiter, Phys. Rev. B **38**, 9545 (1988).

[26] J. Maier, Ber. Bunsenges. Phys. Chem. **90**, 26 (1986).

[27] X. Guo, Solid State Ionics **99**, 137 (1997).

[28] H. Weigand, W. Sprengel, R. Rower, H. E. Schaefer, T. Wejrzanowski, and M. Kelsch, Appl. Phys. Lett. **84**, 3370 (2004).

[29] U. Meyler and P. J. Simpson, Phys. Rev. B **56**, 14303 (1997).

[30] X. Guo, Solid State Ionics **96**, 247 (1997).

[31] X. Guo, Comput. Mater. Sci. **20**, 168 (2001).

[32] X. Guo and Z. Zhang, Acta Mater. **51**, 2359 (2003).